KSME

Springer

Journal of Mechanical Science and Technology 34 (10) 2020

Original Article
DOI 10.1007/s12206-020-0923-8

Keywords:
· Gas turbine combined cycle
· Oxygen injection
· Performance analysis
· Power to methane
· Steam injection

Correspondence to:
Tong Seop Kim
kts@inha.ac.kr

Citation:
Won, D. H., Kim, M. J., Lee, J. H., Kim, T. S. (2020). Performance characteristics of an integrated power generation system combining gas turbine combined cycle, carbon capture and methanation. Journal of Mechanical Science and Technology 34 (10) (2020) 4333~4344.
http://doi.org/10.1007/s12206-020-0923-8

Received January 15th, 2020
Revised July 7th, 2020
Accepted July 28th, 2020

† Recommended by Editor
Yong Tae Kang

Performance characteristics of an integrated power generation system combining gas turbine combined cycle, carbon capture and methanation

Dong Hyeok Won[1], Min Jae Kim[1], Jae Hong Lee[1] and Tong Seop Kim[2]

[1]Graduate School, Inha University, Incheon 22212, Korea, [2]Dept. of Mechanical Engineering, Inha University, Incheon 22212, Korea

Abstract This study analyzes the performance of an integrated power generation system that combines a gas turbine combined cycle (GTCC) with a methanation process. The methanation process uses hydrogen provided by a power-to-gas (PtG) process and carbon dioxide captured from the exhaust gas of the GTCC. The research aim was to maximize the GTCC performance through an effective integration between the GTCC and methanation. Two methods were proposed to utilize the steam generated from the methanation process. One was to supply it to the steam turbine bottoming cycle of the GTCC, and the other was to inject it into the GT combustor. Also investigated was the injection of oxygen generated in the PtG process into the gas turbine combustor. The largest improvements in the power and efficiency were predicted to be 19.3 % and 4.9 % through the combination of the steam supply to the bottoming cycle and the oxygen injection to the combustor.

1. Introduction

The use of renewable energy is increasing rapidly because of escalating concerns about global warming and air pollution. Worldwide renewable power capacity is expected to increase by 1200 GW(50 %) between 2019 and 2024 [1]. Most of the increase in renewable energy is in solar and wind power. Solar photovoltaic (PV) energy alone accounts for almost 60 % of the expected growth and onshore wind power accounted for one quarter. However, solar and wind power is intermittent and fluctuates, whereas the electric energy in a conventional power system is controllable. Hence, the power grid might become unstable as the capacity of renewable energy increases in electric power grids. One solution is to store a large part of the generated renewable energy in energy storage systems (ESSs) to supply it stably to the power grid [2].

To select an appropriate ESS, many options including type selection, optimal sizing, and control strategy should be considered [3]. Various ESSs are being installed and operated, including batteries, but most of them are not practical for storing large amounts, and there are usually discrepancies between the locations of demand and generation. On the other hand, the power-to-gas (PtG) is appropriate for seasonal storage. Furthermore, energy stored with the PtG can be distributed any time and in any place if conventional power plants need to produce more electricity [4].

PtG stores hydrogen by electrolyzing water using renewable energy. The electrolysis techniques used in the PtG process include alkaline electrolysis (AEC) and polymer electrolyte membrane electrolysis (PEMEC), which are low-temperature types, as well as solid oxide electrolysis (SOEC), which is a high-temperature type [5]. AEC is the most mature and low cost technology [6] and PEMEC has higher flexibility and faster cold-start characteristics than AEC [7]. SOEC has higher efficiency than the low-temperature types but it is still in the research-and-development stage [8].

PtG can play different roles in various energy systems. Operators can determine the role of

the PtG using appropriate assessments such as techno-economics, life cycle assessment and multi-criteria decision analysis [9]. Ferrero et al. [10] assessed the cost of the final product when hydrogen is employed for fuel cells and Burkhardt et al. [11] evaluated the environmental impact related to the production of hydrogen and its dispensing to state-of-the-art fuel cell electric vehicles. Guandalini et al. [12] proposed a system integrating PtG with gas turbines by injecting hydrogen into the natural gas grid, showing that the integrated system improved the dispatchability of wind energy by flexible operation of the gas turbines.

The hydrogen generated by PtG can be either supplied to the gas grid or used as fuel of power and energy systems directly or after being reformed. Also, there are many efforts to convert the hydrogen to others. In particular, attempts are being made to convert the hydrogen into synthetic natural gas (SNG) through methanation process for more convenient use of the hydrogen in conventional power generation systems. The integrated technology combining the PtG process and methanation process is called a power-to-methane (PtM).

PtM was first proposed for recirculating the carbon generated from coal-fired thermal power plants in 1994 [13], and a pilot plant was established in 2003 [14]. A 6-MW pilot PtM plant was first installed in Werlte, Germany, in 2014 [15]. The PtM is currently used a lot in Europe, where the penetration of renewable energy is high. It has been investigated extensively in Germany in particular, and many PtM plants are in operation [16]. Bailera et al. [17] researched how to size and manage a cogeneration system that combines PV, PtG, and an oxy-fuel boiler. Blanco et al. [18] expected the enormous potential of PtM in the EU energy transition to a low carbon system in 2050. Various projects have been performed in the US as well, and several PtM-related studies have been conducted. One example is a PtM pilot plant that is being operated on a college campus to supply electricity [19].

Methane is the primary component of SNG generated by the methanation process and can be supplied to the natural gas grid because its properties are highly similar to those of natural gas. Therefore, the integration system of PtM and conventional power plants, such as gas turbines, could be a solution to the variability of renewables. Gas turbines have secured the position of a major power source during the past decades. The reason for the rapid growth is their high thermal efficiency. Furthermore, high operational flexibility is another important factor. In particular, their capability of high ramp-rate and fast start-up for high cycling duty is a very important advantage in modern dynamic electric power grids. Therefore, the future of gas turbines is also bright because the growth of renewable energy would naturally require rapid-responding power sources to compensate for the intermittency of the power generation from renewable sources [20, 21].

In this respect, the integration of gas turbines with PtM could be a future-oriented research topic. However, although a lot of studies on the PtM have been presented recently as summarized above, only a few studies have been performed on the integration of the PtM with gas turbines. Sterner [22] proposed the idea of integration but did not analyze the performance in detail. Bailera et al. [23] performed a study on the PtM integrated with an oxy-combustion power plant, which is not commercialized yet. Therefore, a detailed analysis on the performance characteristics of the PtM-gas turbine integrated system is required, and we aimed to propose a direct integration of a gas turbine with a methanation process using the hydrogen from PtG as fuel for the GTCC.

The carbon dioxide in the exhaust gas from the gas turbine is captured and used for the methanation process. Actually, the power system is not a simple gas turbine but a gas turbine combined cycle (GTCC) which combined a gas turbine and a steam turbine. The aim of our study was to evaluate the thermodynamic performance of the directly integrated system, which has not been conducted until now. Prakash and Singh [24] suggested an idea of combining the GTCC with PtM. However, the produced methane in their system was not used directly for the GTCC but used for a GT which was installed separately. In our study, the methane from the PtM process is directly used as fuel of the GTCC, partially replacing the natural gas fuel. In addition to suggesting a new integrated power plant system, we proposed two methods to maximize the performance of the integrated system. Firstly, the steam generated from the methanation process is injected into the gas turbine's combustor. Next, the oxygen generated from the PtG process is injected into the inlet of the gas turbine combustor. Performance improvement in each method were comparatively analyzed.

Table 1. Definition of cases.

Case 1	GTCC + CCS + methanation (steam supply to bottoming cycle)
Case 2	GTCC + CCS + methanation (steam injection at combustor)
Case 3	GTCC + CCS + methanation (steam supply to bottoming cycle) + oxygen injection

2. Configuration and modeling

2.1 Case definition

Three cases of designing the system, defined in Table 1, were compared. Case 1 combines a carbon capture process (CCP) and a methanation process (MP) with a GTCC, as illustrated in Fig. 1. Our simulation did not include the PtG process that generates the hydrogen because our research focus was given to the utilization of syngas from methanation, and it was assumed that the required hydrogen was purchased from the PtG operator (i.e. the hydrogen producer).

The GTCC system was designed based on the TITAN 130 from Solar Turbines, Inc., which is a 15-MW class gas turbine that is applicable to distributed power generation. A dual or triple-pressure steam bottoming cycle is not economical for small gas turbines, so a single-pressure heat-recovery steam

Table 2. Design specifications of the gas turbine.

Components	Parameters	Reference	Simulation	
Compressor	Pressure ratio	17.1	17.1	Input
	Isentropic efficiency [%]	83	83	Input
Combustor	Fuel flow rate [kg/s]	N/A	0.862	Calculated
	Pressure loss [%]	N/A	4	Assumed input
Turbine	Isentropic efficiency [%]	N/A	91.7	Calculated
	Firing temperature [°C]	1177	1177	Input
	Turbine exhaust temperature [°C]	496	496	Input
	Turbine inlet mass flow [kg/s]	49.8	49.8	Input
Performance	Mechanical efficiency [%]	N/A	97.6	Assumed input
	Gear box efficiency [%]	N/A	96.6	Assumed input
	Generator efficiency [%]	N/A	96.0	Assumed input
	Net power [MW]	15	15	Input
	Net efficiency [%]	35.2	35.2	Input

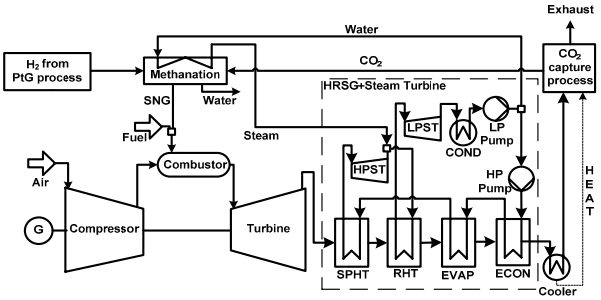

Fig. 1. Configuration of case 1.

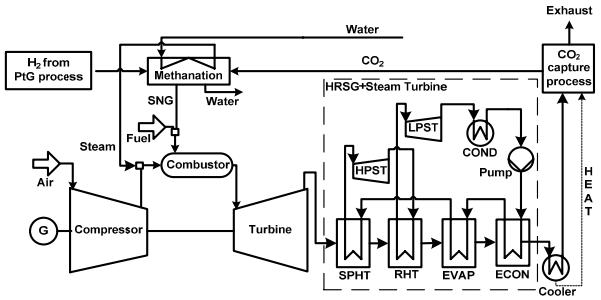

Fig. 2. Configuration of case 2.

generator (HRSG) was adopted. To maximize the power output of the bottoming cycle, the steam turbine was divided into two sections, a high pressure steam turbine (HPST) and a low pressure steam turbine (LPST), and a reheater was installed between them.

The thermal energy required in the CCP is supplied by the exhaust gas of the GTCC, which is explained in more detail in Sec. 2.3. The carbon dioxide captured by the CCP was used in the methanation process, and the SNG generated by methanation was used as the fuel for the gas turbine. The methanation process generates heat, which is used to produce steam. This steam is supplied to the outlet of the HPST to increase the net power of the bottoming cycle. On the other hand, in case 2 (Fig. 2), the steam was injected into the combustor to increase the net power of the GTCC further by increasing the power of both the gas turbine and bottoming cycle simultaneously.

The oxygen generated from the PtG process is generally sold to consumers. However, it is also possible that the oxygen could be injected into the gas turbine combustor to further increase the power output and efficiency of the GTCC. This idea is reflected in case 3 (Fig. 3). In this system, the steam generated by methanation is supplied to the bottoming cycle, as in case 1. It was also assumed that oxygen is purchased from the PtG operator as with the hydrogen.

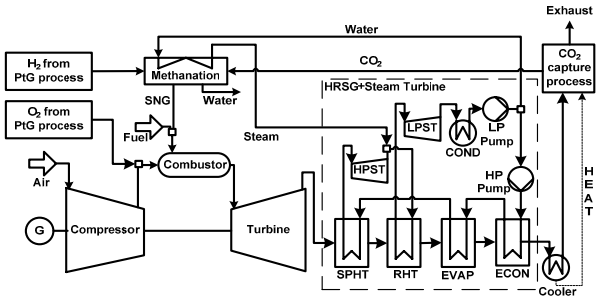

Fig. 3. Configuration of case 3.

2.2 System modeling

2.2.1 Design specifications of the gas turbine combined cycle

The gas turbine simulation was performed using in-house code [25] that was developed in MATLAB [26]. The performance of the Titan 130 was simulated using the specifications from the Ref. [27]. The gas turbine modeling explained in this section is rather brief for the sake of the compactness of this paper. Details of the modeling can be referred to Ref. [25]. The design specifications of the gas turbine are outlined in Table 2. ISO conditions were used for the ambient air (1 atm, 15 °C). The natural gas included 89.0 % CH_4, 8.7 % C_2H_6, 1.7 % C_3H_8,

and other hydrocarbons. The lower heating value (LHV) was 49426 kJ/kg.

The flow rate of natural gas was calculated from the net power, efficiency, and the LHV of the fuel. The turbine efficiency was determined using the known turbine exhaust temperature (TET). The net power and efficiency of the gas turbine were defined using Eqs. (1) and (2), respectively. The results of the design analysis accurately coincided with the net power, efficiency, and turbine outlet temperature in the specification data.

$$\dot{W}_{GT} = \left(\dot{W}_{Turb} - \dot{W}_{Comp}\right)\eta_{mech}\eta_{gear}\eta_{gen} \quad (1)$$

$$\eta_{GT} = \frac{\dot{W}_{GT}}{\left(\dot{m} \times LHV\right)_{NG}}. \quad (2)$$

Aspen HYSYS [28] was used for the performance analysis of the steam turbine bottoming cycle. The properties and composition of the gas turbine's exhaust gas obtained from the gas turbine simulation were input into HYSYS, and the bottoming cycle performance was calculated [29]. The primary design parameters of the bottoming cycle are listed in Table 3. The table also shows the simulated performance of the GTCC plant. The HPST inlet pressure was set to 41.5 bar referring to the design data of an actual GTCC plant that uses the gas turbine adopted in this study [30]. The isentropic efficiency was assumed to be 89 % for both turbines.

The HRSG is composed of four heat exchangers: an economizer (ECON), evaporator (EVAP), superheater (SPHT), and reheater (RHT). Each one was assumed to be a counter-flow heat exchanger. The design performance was simulated using the energy balance equation in Eq. (3), and the net power of the bottoming cycle was defined using Eq. (4) [31].

$$\dot{m}_g\left(h_{g,in} - h_{g,out}\right) = \dot{m}_s\left(h_{s,out} - h_{s,in}\right) \quad (3)$$

$$\dot{W}_{ST} = \left(\sum \dot{W}_{ST}\right)\eta_{gen} - \left(\sum \dot{W}_p\right)/\eta_{mo}. \quad (4)$$

The net power and efficiency of the GTCC are defined using Eqs. (5) and (6), respectively.

$$\dot{W}_{CC} = \dot{W}_{GT} + \dot{W}_{ST} \quad (5)$$

$$\eta_{CC} = \frac{\dot{W}_{CC}}{\left(\dot{m} \times LHV\right)_{NG}}. \quad (6)$$

The net power of the gas turbine in the GTCC plant is less than that of the standalone mode (GT-alone) by 2.9 % because there is additional pressure loss at the HRSG: 5 % pressure loss in the HRSG was assumed. The additional pressure loss causes the turbine exit pressure to rise. This decreases the expansion ratio of the turbine, which reduces the turbine power production. The predicted steam turbine power was 6.28 MW. The net GTCC power and efficiency were 20.9 MW and 48.9 %.

Table 3. Bottoming cycle design parameters and GTCC performance.

Components		Parameters	Simulation
Bottoming cycle	Condenser	Pressure [bar]	0.04
		Steam flow rate [kg/s]	3.53
	HPST	Inlet pressure [bar]	41.5
		Inlet temperature [°C]	456
	LPST	Inlet pressure [bar]	2.56
		Inlet temperature [°C]	410
	ST	Isentropic efficiency [%]	89
		Generator efficiency [%]	96.0
	Pump	Motor efficiency [%]	95.0
	HRSG	Pinch point temperature [°C]	10
		Exhaust temperature [°C]	170
	Performance	Net power [MW]	6.28
GTCC	Performance	Net power [MW]	20.85
		Net efficiency [%]	48.9

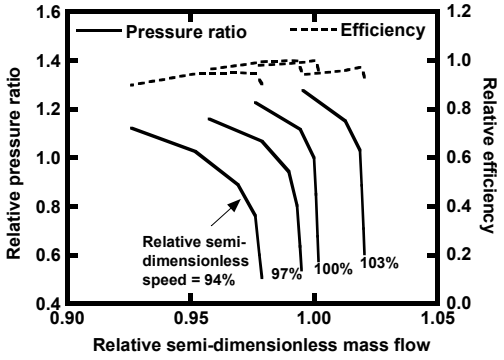

Fig. 4. Normalized compressor map.

2.2.2 Off-design model of the gas turbine combined cycle

The gas turbine operates in off-design conditions when SNG is used as the primary fuel instead of natural gas (which the gas turbine is designed for) and when oxygen or steam is injected. Furthermore, the bottoming cycle also operates in off-design conditions due to the variations in the exhaust gas conditions such as the temperature, composition, and flow rate. Therefore, a full off-design simulation was required for the entire GTCC system. A compressor map [32] with similar design performance was corrected and used to reproduce the off-design performance data that have been released for the target gas turbine [33]. The compressor map used in the simulation is shown in Fig. 4, where all the parameters are normalized using design values. Actually, the mass flow rate and speed were expressed as a relative semi-dimensionless parameter as follows.

$$\text{Relative semi-dimensionless mass flow: } \frac{\left(\frac{\dot{m}\sqrt{PT}}{P}\right)_{in}}{\left(\frac{\dot{m}\sqrt{PT}}{P}\right)_{in,d}} \quad (7)$$

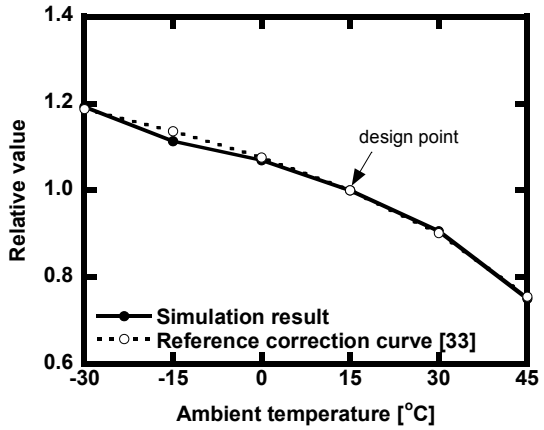

Fig. 5. Comparison of variation in power output with ambient temperature between simulation and manufacture's correction curve.

$$\text{Relative semi-dimensionless speed: } \frac{\left(\frac{N}{\sqrt{RT}}\right)_{in}}{\left(\frac{N}{\sqrt{RT}}\right)_{in,d}}. \quad (8)$$

In general, turbine inlet can be assumed to be in a choking state. Therefore, the choking Eq. (9), which is widely used for industrial gas turbines, was used as the off-design model of the gas turbine [34].

$$\left(\frac{\dot{m}_{in}\sqrt{T_{in}}}{\kappa A_{in} P_{in}}\right)_T = const, \quad \kappa = \sqrt{\frac{\gamma}{R}\left(\frac{2}{\gamma+1}\right)^{\frac{\gamma-1}{\gamma+1}}}. \quad (9)$$

The off-design models of the gas turbine were validated through a comparison of the predicted off-design performance results with the manufacture's data. Fig. 5 illustrates an example of the good agreement of the predicted variation in the full load power output of the target engine with that of the manufacturer's correction curve [33].

When additional flow is injected into the combustor, the flow rate of the turbine increases, and the pressure ratio of the compressor increases due to the operation matching of the compressor and turbine [35]. Accordingly, when steam or oxygen is injected into the combustor, the pressure ratio of the compressor also increases. This implies that the compressor operation point moves toward the surge point. For safe operation of the compressor, it is necessary to move away sufficiently from the surge point. Hence, the surge margin must be predicted using the following equation:

$$\text{Surge margine} = \frac{PR_{Surge} - PR_{operation}}{PR_{operation}} \times 100(\%). \quad (10)$$

The effectiveness-NTU method was applied in the off-design analysis of the heat exchangers of the HRSG. At the design point, the effectiveness of each heat exchanger was calculated according to Eq. (11) using all the temperature data which were outcomes of the thermodynamic analysis. Then, the design values of the *NTU* and *UA* were calculated by Eqs. (12) and (13). Eq. (12) was for the evaporator in which a phase change occurs and Eq. (13) was for all the other heat exchangers [36]. In the off-design state, the *UA* of each heat exchanger was corrected using Eq. (14), which represents the dependence of the UA with flow rate [32]. An index of 0.8 was adopted from the Dittus-Boelter correlation [36]. Then, the NTU and effectiveness at the off-design state were evaluated using Eqs. (12) and (13). Finally, the outlet temperatures of both the hot and cold side of each heat exchanger were predicted by Eq. (11).

$$\varepsilon = \frac{C_h\left(T_{h,in} - T_{h,out}\right)}{C_{\min}\left(T_{h,in} - T_{c,in}\right)} \text{ or } \frac{C_c\left(T_{c,out} - T_{c,in}\right)}{C_{\min}\left(T_{h,in} - T_{c,in}\right)} \quad (11)$$

$$\text{where, } C = \dot{m}c_p$$

$$NTU = \frac{UA}{C_{\max}} = -\ln(1-\varepsilon) \quad (12)$$

$$\text{where, } C_r = \frac{C_{\min}}{C_{\max}} = 0$$

$$NTU = \frac{UA}{C_{\min}} = \frac{1}{C_r - 1}\ln\left(\frac{\varepsilon - 1}{\varepsilon C_r - 1}\right) \quad (13)$$

$$\text{where, } C_r = \frac{C_{\min}}{C_{\max}}$$

$$UA = (UA)_d\left(\frac{\dot{m}}{\dot{m}_d}\right)^{0.8}. \quad (14)$$

Stodola's ellipse law was used for the off-design analysis of the steam turbines [37]. The turbine inlet pressure in the off-design conditions was calculated by the following equation:

$$\frac{\Phi}{\Phi_d} = \frac{\sqrt{1-\left(\frac{P_{out}}{P_{in}}\right)^2}}{\sqrt{1-\left(\frac{P_{out}}{P_{in}}\right)^2_d}}, \quad \text{where } \Phi = \left(\frac{\dot{m}\sqrt{T}}{P}\right)_{in}. \quad (15)$$

2.2.3 Carbon capture process

CO_2 is captured from the GTCC exhaust gas. In the capture process, CO_2 is removed using an absorbent such as monoethanolamine (MEA) or selexol. A CCP model with MEA as an absorbent was adopted based on the work of Øi et al. [38]. A diagram of the CCP which consists of the MEA process and CSU is shown in Fig. 6, and their design values are listed in Table 4. Aspen HYSYS was used for the CCP analysis as well. The CO_2 capture rate of the MEA process was set as 85 %. The GTCC exhaust gas flows into the absorber inlet at 40 °C after two cooling steps. The number of stages of the absorber and desorber and the Murphee efficiency were referenced from the Ref. [31].

Table 4. Design parameters of MEA process and CSU.

Components	Parameters	Value
MEA process	Capture rate [%]	85
	Inlet gas temperature [°C]	40
	Number of stages in absorber	10
	Murphree efficiency in absorber	0.25
	Desorber temperature [°C]	120
	Number of stages in desorber	6
	Murphree efficiency in desorber	1.0
CSU	CO_2 compressor pressure [kPa]	3000
	Cooler outlet temperature [°C]	25
	Compressor isentropic efficiency [%]	95

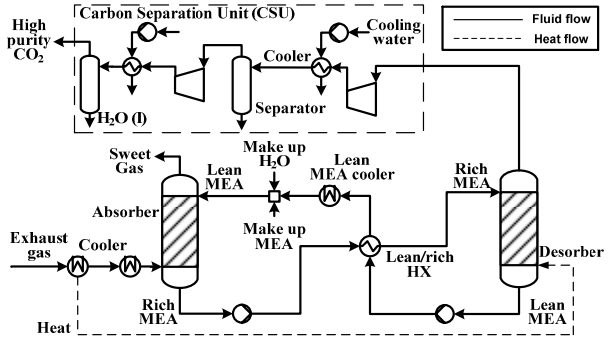

Fig. 6. Configuration of the carbon capture process.

The CSU consists of two compression and condensation processes. Consequently, the captured CO_2, which has 99.6 % purity, is stored as a gas at 30 bar and 40 °C. This gas is supplied to the methanation process. The design values of the CSU were taken from Li and Yan [39]. The overall CO_2 capture rate of the total plant is defined as the flow rate of the carbon dioxide captured by the CCP in the total carbon dioxide flow rate of the exhaust gas of the GTCC as shown in the following equation:

$$CR = \frac{\dot{m}_{CO_2,captured}}{\dot{m}_{CO_2,generated}}. \quad (16)$$

The total power consumption of the CCP is calculated by the following equation:

$$\dot{W}_{CCP} = \dot{W}_{MEA} + \dot{W}_{CSU} = \sum \dot{W}_{P,MEA} + \sum \dot{W}_{Comp,CSU} + \sum \dot{W}_{P,CSU}. \quad (17)$$

2.2.4 Methanation process

The theoretical chemical equation of the methanation is shown in Eq. (18). The ideal mole ratio of hydrogen to carbon dioxide is 4:1.

$$CO_2 + 4H_2 \rightarrow CH_4 + 2H_2O \quad (18)$$

Table 5. Design parameters of methanation process.

	Pressure [bar]	Temperature [°C]	CH_4 mole fraction [%]
H_2	30.0	15.0	N/A
CO_2	30.0	40.0	N/A
R1 inlet	30.0	308	15.8
R1 outlet	29.5	594	24.8
R2 inlet	28.6	250	24.8
R2 outlet	28.2	411	30.6
R3 inlet	27.0	250	72.6
R3 outlet	26.8	376	81.2
SNG	26.3	40.0	95.0

Methanation processes can be divided into catalytic methanation and biological methanation. Biological methanation operates at 30-60 °C and atmosphere pressure but suffers from low mass transfer and flexibility [40]. Therefore, catalytic methanation was considered in this study. The most important factor in the catalyst process is temperature. If the temperature of the reactor is lower than 250 °C, the catalyst reaction does not occur, but if it is higher than 550 °C, a reverse reaction occurs. Therefore, the operation temperature of the reactor must be set between 250 and 550 °C [41]. Various reactors are used in the catalyst process, but an adiabatic or isothermal reactor is used primarily. The SNG that contains a considerable amount of methane can be obtained with only one isothermal reactor, but a complex channel is required, which makes the isothermal reactor very expensive. The channel design of the adiabatic reactor is easier than that of an isothermal reactor, but more than one reactor must be used [42].

The TREMP™ process from Haldor Topsøe for the adiabatic reactor was referenced [23], and the required design values are listed in Table 5. The configuration of the process is shown in Fig. 7, where the solid line indicates the fluid flow, and the dotted line indicates the heat flow. Aspen HYSYS was used for the analysis, and the design parameters of each component are listed in Table 5. Inside the adiabatic reactor, a reaction occurs to minimize the Gibbs free energy. After the first reactor, approximately 72.5 % of the total flow rate can be recirculated to reduce the number of adiabatic reactors. After the second and third reactors, the generated water is removed by a condenser. In the methanation process, electric energy is consumed in the operation of a blower that is required for the recirculation of the working fluid.

As a result of the analysis, SNG containing 95.0 % methane, 4.0 % hydrogen 0.6 % CO_2 and 0.4 % H_2O by volume was obtained. The LHV of SNG is 49260 kJ/kg, which is slightly lower than that of the natural gas. The efficiency of the methanation process is defined by Eq. (19). The analysis result indicated an efficiency of approximately 83.1 %, which is within the range reported previously [22].

$$\eta_{MP} = \frac{\dot{m}_{SNG} \times LHV_{SNG}}{\dot{m}_{H_2} \times LHV_{H_2}}. \quad (19)$$

Steam was produced using the heat generated by the methanation process. According to the referenced TREMP™ process [23], the inlet temperature of each reactor (R1, R2 and R3) needs to be maintained constant to guarantee a target production rate of SNG. Therefore, in our modeling, the hot side outlet temperature of each heat exchanger (HEX2, HEX3 and HEX4) was maintained to be constant. The simulated SNG production rate was almost the same as that of the Ref. [23], which validated our modeling. The temperature of the produced steam was determined from the flow rate of the steam. If the steam flow rate decreases, it could be impossible to recover the heat in the process because the temperature of the cold side increases. Conversely, if the flow rate of steam increases, it might be in a two-phase liquid-vapor mixture state because the outlet temperature of the cold side decreases. Therefore, the steam flow rate is limited to a certain range. The steam is supplied into the bottoming cycle (cases 1 and 3) or injected into the gas turbine combustor (case 2). In each case, the change in performance in the GTCC system combined with the methanation process was analyzed for changes in flow rate within a range limited by physical boundary conditions.

2.3 Operation strategy

The GTCC system combined with the methanation process has the following operation sequence. First, carbon dioxide is captured through the CCP from the exhaust gas of the GTCC. Thermal energy is required to heat the MEA solution of the CCP desorber. In the case of a large GTCC, the heat is generally supplied by the steam drawn from the middle stage of the steam turbine [30]. If this method were adopted, the HPST outlet steam would have to be used. However, the gas turbine used in this study is small, so the exhaust gas temperature is lower than that of a large gas turbine. Moreover, the heat recovery rate of the HRSG is lower than that of the large GTCC because the HRSG is the single-pressure type. Therefore, if steam is supplied from the HPST outlet, enough heat cannot be supplied for the MEA process. As an alternative, the exhaust gas that passes through the HRSG was used as a heat source. The first cooler in Fig. 6 was installed for this purpose. The second cooler was adopted to fix the absorber inlet gas temperature at 40 °C. The temperature of the GTCC exhaust gas at the HRSG exit (i.e. the temperature of the incoming exhaust gas in Fig. 6) was set as 270 °C to supply sufficient heat to the MEA solution at the desorber. Because of this measure, the net power of the bottoming cycle inevitably decreases.

All of the carbon dioxide captured by the CCP was used in the methanation process. The molar flow rate of hydrogen required for the methanation process was determined in proportion to the molar flow of carbon dioxide. This hydrogen is received (or purchased) from the PtG. The SNG produced from the methanation process were used as fuel for the gas turbine. However, natural gas was additionally supplied because the flow rate of the produced SNG was 16-18 % lower than the fuel flow rate required to maintain the firing temperature at the design value (1177 °C).

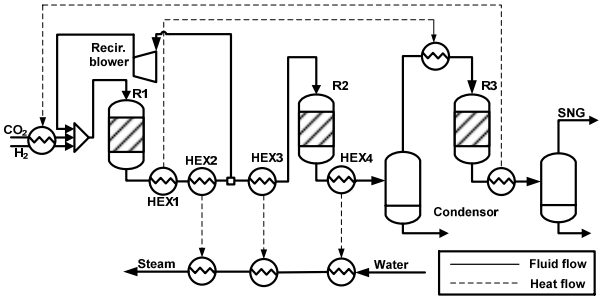

Fig. 7. Scheme of the TREMP™ methanation process.

Steam was injected into the combustor in case 2, and oxygen was injected in case 3. The pressure of the injected steam and oxygen was set as 1.2 times the inlet pressure of the combustor so that they could be injected smoothly. The minimum surge margin for stable compressor operation was assumed to be approximately 10 %. The maximum flow rates of the injected oxygen were then determined. It was assumed that up to 6 kg/s of oxygen (12.5 % of the compressor inlet air) could be injected into the combustor. The net power and efficiency of the total system were defined as follows:

$$\dot{W}_{net} = \dot{W}_{GT} + \dot{W}_{ST} - \dot{W}_{CCP} - \dot{W}_{MP} \quad (20)$$

$$\eta_{net} = \frac{\dot{W}_{net}}{(\dot{m} \times LHV)_{H_2} + (\dot{m} \times LHV)_{NG}}. \quad (21)$$

3. Results and discussion

3.1 Performance outline

Table 6 summarizes the performance specification of the optimal design condition of each case, which was selected as a result of a parametric analysis on the major design variables. The process and result of the parametric analysis will be explained in the next three sections. Before we proceeded to the detailed examination of the results, we checked the compatibility of the syngas fuel with the natural gas which is the design fuel of the gas turbine.

The Wobbe index defined by Eq. (22) is generally used to compare the combustion energy of various fuel gases. Using this index, we can determine the possibility of using the SNG produced from the methanation process in the gas turbine combustor.

$$\text{Wobbe index} = HHV_{mix} / \sqrt{SG_{mix}}. \quad (22)$$

We assumed that the proposed technology can best be disseminated in Europe because the renewable energy penetration in electric power grids is high in Europe. The Wobbe index

Table 6. Performance analysis results.

Parameters	Case 1	Case 2	Case 3
Supplied steam mass flow [kg/s]	2.8	N/A	3.0
Injected steam mass flow [kg/s]	N/A	3.6	N/A
Injected oxygen mass flow [kg/s]	N/A	N/A	6.0
Natural gas mass flow [kg/s]	0.151	0.171	0.171
Hydrogen mass flow [kg/s]	0.366	0.417	0.416
SNG mass flow [kg/s]	0.734	0.837	0.838
Compressor pressure ratio	17.1	18.7	19.0
Compressor inlet flow rate [kg/s]	48.9	48.7	48.7
Exhaust gas flow rate [kg/s]	49.8	53.3	55.6
HPST inlet mass flow [kg/s]	3.70	4.30	3.89
Surge margin [%]	21.2	10.9	9.33
GT power [MW]	14.70	18.87	18.31
ST power [MW]	6.75	5.61	7.24
CCP power consumption [MW]	0.64	0.74	0.73
MP power consumption [MW]	0.08	0.09	0.09
Net system power [MW]	20.73	23.64	24.73
Net system efficiency [%]	40.66	40.74	42.67

of SNG was 14.57 kWh/Nm^3, which is within the index range of natural gas supplied in Europe [43]. Therefore, the combustor can be used without modification even though it was designed for standard natural gas.

The LHV of the SNG was slightly lower than that of the natural gas. Therefore, the flow rate of the total amount of fuel supplied to the combustor is slightly higher than that of the deign state in all cases because the TIT is controlled to be constant at the design value. Due to the increase of the gas mass flow rate in the turbine as a result of the increased fuel flow rate, the GT power increases slightly in comparison to the design state. Both the net power output and efficiency were the highest in case 3. The next three sections describe the performance characteristics of each case and a comparison among them.

3.2 Case 1: gas turbine combined cycle integrated with carbon capture and methanation process

The major design variable is the steam flow rate produced in the methanation process. There are upper and lower limits of the steam flow rate. The steam generated from the methanation process is mixed with the exiting steam from the HPST (see Fig. 1). Thus, the pressure of the generated steam is fixed at the HPST outlet pressure. The temperature of the steam should also be lower than the HEX2 inlet temperature which is 577 °C (see Fig. 7). At a fixed pressure, the lower flow rate is, the higher the steam temperature becomes. The lowest possible flow rate was 2.8 kg/s. When the flow rate becomes too high, steam begins to condense. The upper limit to avoid condensation was 3.6 kg/s. As a result, the possible range of the steam flow rate was between 2.8 kg/s and 3.6 kg/s.

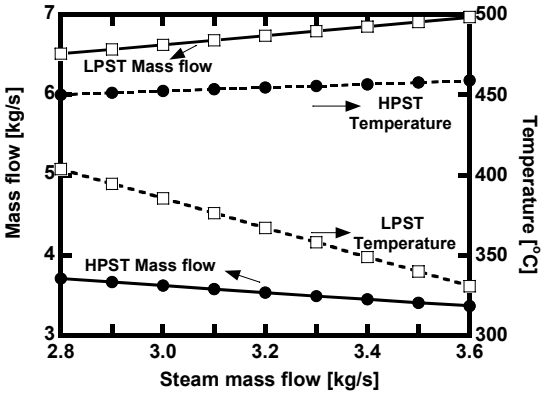

Fig. 8. Variations in steam turbine inlet conditions with the flow rate of steam generated by the methanation process and supplied to the steam turbine in case 1.

Fig. 8 is the result of the parametric analysis. It shows the changes in inlet flow rates and temperatures of the HPST and LPST according to the flow rate of steam supplied by the methanation process. A higher flow rate of steam generated in the methanation process results in a lower temperature of the produced steam. Therefore, a higher flow rate of supplied steam results in a higher flow rate at the LPST inlet but a lower inlet temperature.

The power of the LPST decreased as the supplied flow rate increased because the inlet temperature decreased significantly, while the increase in the flow rate of the LPST inlet was relatively small. Furthermore, the power of the HPST decreased as the flow rate of the supplied steam increased. The increase in the flow rate of the LPST inlet resulted in higher heat recovery for RHT and lower heat recovery for EVAP. Therefore, a higher flow rate of the supplied steam led to a lower inlet flow rate of the HPST, and it reduced the HPST power.

Therefore, the power increase was the biggest when the steam flow rate was 2.8 kg/s, which was the lower limit. So, this point was selected as the optimal design condition, the result of which was listed in Table 6. At the design condition, the amount of carbon dioxide captured using the CCP from the exhaust gas of the GTCC was 2.13 kg/s, and the amount of hydrogen used in the methanation process was 0.366 kg/s. The methanation process generated SNG at 0.734 kg/s, and the mole fraction of methane was 95.0 %. The additional natural gas flow rate was 0.151 kg/s. Thus, the net fuel flow rate to the GT combustor was 0.885 kg/s. which was 0.12 % higher in comparison to the design state leading to 2.7 % higher GT power. The surge margin was 21.2 %, which is 0.2 %p lower than the design value. But the reduction was quite marginal.

The net power of the steam turbines was 6.75 MW, which was 7.5 % increase from the reference power of 6.28 MW (see Table 3). The sum of the gas turbine and steam turbine powers were larger than that of the design state. When including the CCP and MP power consumptions, the net system power output was predicted to be 20.73 MW, which was almost compa-

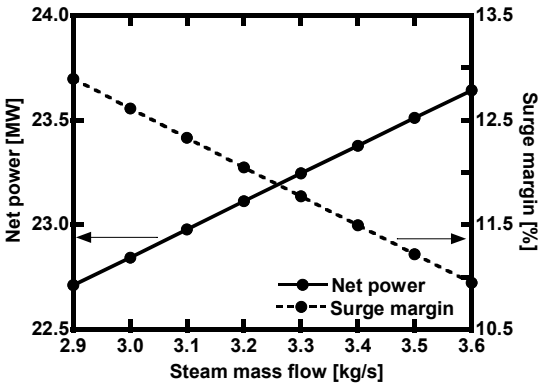

Fig. 9. Net system power and compressor surge margin with respect to the injected steam flow rate in case 2.

rable to that of the design state (20.85 MW). The net system efficiency was 40.66 %.

The decrease in the system efficiency from that of the design state is quite natural because the energy consumption in both the carbon capture and methanation processes was taken into account in the efficiency calculation of the PtM-GTCC combined system. However, a direct comparison of the two efficiencies has a limited value because the raw fuels are different. The major fuel was the hydrogen from the PtG process in the PtM-GTCC combined system, while the entire fuel is the natural gas in the conventional GTCC. Therefore, instead of putting an excessive importance on the absolute value of the efficiency drop from the conventional GTCC, it is more reasonable to make an effort to improve the system configuration further to achieve the highest possible efficiency of the PtM-GTCC combined system. So, the target of our study was set at maximizing the gas turbine power output of the integrated PtM-GTCC system, which in turn minimizes the efficiency penalty. In this respect, case 1 was used as a reference case and two revised cases were proposed in search of the possibility of further performance enhancement.

3.3 Case 2: steam injection

The major design variable in case 2 was also the flow rate of the steam produced in the methanation process. Because all of the produced steam was injected into the GT combustor, the variable will be called the flow rate of the injected steam in this section.

Fig. 9 shows the variation in the net power output according to the flow rate of injected steam. The principle of selecting the lower limit of the steam flow rate was similar to that explained in the last section. The pressure of the generated steam was set at 1860 kPa, which was slightly higher than the compressor exit air pressure, because it should be injected into the compressed air. The temperature of the generated steam was controlled by the HEX2 inlet temperature (see Fig. 7) as was the case in the last section. The lowest steam generation rate to satisfy this temperature limit was 2.9 kg/s.

The upper limit of the injected steam flow rate was posed by the surge margin of the compressor. As the injected steam flow rate increases, the turbine inlet flow rate increases, leading to increase in net power output of the GT. However, an increase in the injection flow rate increases the operating pressure ratio of the compressor, leading to a reduction in the surge margin. With 3.6 kg/s of steam injection, the pressure ratio increased by 1.6 (9.4 %), and the surge margin decreased by 10.3 %p, reaching the assumed minimum allowable value. The steam temperature decreases with increasing steam flow rate in the methanation process as was explained in case 1. Therefore, the flow rate of the fuel added to maintain the TIT of the gas turbine increases as the injected steam flow rate increases. Because the increase in fuel flow is dominant over the increase in power, net efficiency decreases as the injected steam flow rate increases. It was not easy to determine an optimal design steam flow rate because of the reversed trends of the power and efficiency. However, we selected the maximum steam flow condition (3.6 kg/s) as the nominal design condition because the rate of efficiency increase with decreasing steam flow rate is higher than the rate of power decrease.

With 3.6 kg/s of steam injection, the net power of the gas turbine increased by 4.2 MW (28.6 %) compared to case 1, as shown in Table 6. The power of the HPST increased by 0.45 MW compared to case 1. In contrast, the flow rate of the LPST decreased, and the power of the LPST decreased by 1.52 MW. Therefore, the total power of the steam turbine decreased to 5.61 MW, which is approximately 83 % that of case 1. Consequently, the net system power increased by 2.91 MW (14.0 %) compared to case 1. The increase in the efficiency was marginal (about 0.1 %p).

3.4 Case 3: oxygen injection

In case 3, the steam generated from the methanation process is supplied to the bottoming cycle of the GTCC as in case 1. Therefore, the steam generation rate was determined using the same principle as in case 1. Then, major design variable was the injection flow rate of the oxygen. If oxygen is injected into the GT combustor, the net GT power output increases due to the increased turbine mass flow rate. This is the same reason of the power boost in case 2 where steam was injected. As the oxygen injection rate increases, the net power output increases steadily but the surge margin decreases. Fig. 10 shows the trend. When the oxygen flow rate reached 6 kg/s, the surge margin reduced to 9.3 %, which was very close to the allowable lower limit. Therefore, we selected 6 kg/s as the design oxygen injection rate, and the performance summary at this operating condition was listed in Table 6.

It is clear from Table 6 that the net power output of case 3 is larger than that of case 2: remember that the operating point of case 2 listed in Table 6 was the condition for the largest power generation. The steam generation rate in the methanation process is similar to that of case 1. The slight difference is due to the slight change in heat balance between the two systems.

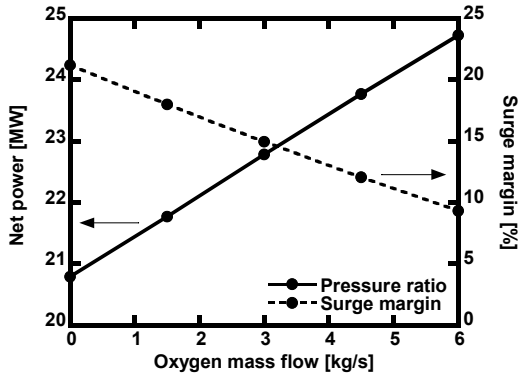

Fig. 10. Net system power and compressor surge margin with respect to the injected oxygen flow rate in case 3.

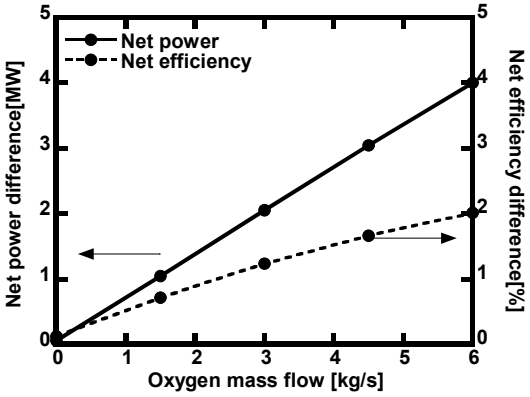

Fig. 11. Performance benefit of case 3 over case 1 with respect to the injected oxygen flow rate in case 3.

The turbine exhaust mass flow was even greater than in case 2, which was favorable in the steam turbine power production. Moreover, the efficiency is also higher in case 3.

Compared to case 1, case 3 increased the net power of the gas turbine and bottoming cycle by 3.6 MW (24.6 %) and 0.43 MW (7 %), respectively. Consequently, the net system power increased by 19 % to 24.73 MW. The injection of oxygen increased the flow rate of fuel by approximately 13 % compared to case 1. The flow rate of the fuel increased as the flow rate of injected oxygen increased. Because the power increase was larger than the increase in fuel flow, the system efficiency increased with increasing oxygen injection rate. Therefore, as the injection rate increases, not only the benefit of power but also that of efficiency over case 1 increase as shown in Fig. 11. At the selected design point of 6 kg/s injection, the efficiency gain over case 1 was predicted to be 2.01 %p (4.9 %).

4. Conclusion

In this study, performance characteristics of an integrated power generation system was analyzed, which generates SNG through methanation using carbon dioxide captured from the GTCC exhaust gas and hydrogen generated by the PtG. The main focus was on the injection of the steam produced by methanation and the oxygen produced by the PtG process into the gas turbine combustor. The goal was to improve the performance of the GTCC system integrated with methanation. The results and conclusion are summarized as follows.

In case 1, the steam flow rate generated in the methanation process was between 2.8 and 3.6 kg/s, and the steam was supplied to the steam turbine bottoming cycle. The power and efficiency of the overall system were the highest when the steam flow rate was the minimum. The optimum power and efficiency were 20.73 MW and 40.66 %, respectively.

In case 2, the steam generated by methanation was injected into the GT instead of being supplied to the bottoming cycle. As the flow rate of the steam injected into the gas turbine increased, the net power increased, but the rate of increase of the efficiency was lower. At the maximum injection flow rate, the net power and efficiency increased by 2.98 MW (14.8 %) and 0.1 %p in comparison to case 1.

In case 3 where the oxygen generated by the PtG process was injected into the GT combustor, the net power and efficiency improved considerably in comparison to case 1. With the maximum injection flow rate of oxygen, the net power and efficiency improved by 4.0 MW (19.3 %) and 2.01 %p (4.9 %), respectively. Case 3 provided the highest power and efficiency among the three cases in which the GTCC was integrated with methanation.

The gas turbine is the most suitable power source to compensate for the variability of renewables. PtG is also expected to play an important role as a large-capacity energy storage device for storing renewable energy. Therefore, integration of GTCC with a methanation process which uses hydrogen produced from PtG would contribute to the stable power supply in the future. Consequently, the result of this study could be the base of further research on the integrated system, for example a thermo-economic analysis.

Acknowledgments

This work was supported by the National Research Foundation of Korea (NRF) grant funded by the Korea government (MOE) (No. 2017R1A2B4006859).

Nomenclature

A : Area (m^2)
CCP : Carbon capture process
C_p : Constant pressure heat capacity (kJ/kg·K)
CR : Capture rate
CSU : Carbon separation unit
h : Enthalpy (kJ/kg)
HHV : Higher heating value (kJ/kg)
HPST : High pressure steam turbine
LHV : Lower heating value (kJ/kg)
LPST : Lower pressure steam turbine
MP : Methanation process
$\dot{m}$: Mass flow rate (kg/s)

N : Rotation speed (RPM)
PR : Pressure ratio
SG : Specific gravity
T : Temperature (K)
U : Overall heat transfer coefficient (kW/m^{2}K)
$\dot{W}$: Power (kW)
ε : Effectiveness
γ : Specific heat ratio
η : Efficiency

Subscript

c : Cold side
CC : Gas turbine combined cycle
CCP : Carbon capture process
Comp : Compressor
d : Design
e : Electricity
hg : Gas
gear : Gearbox
gen : Generator
GT : Gas turbine
h : Hot side
HP : High pressure
in : Inlet
LP : Low pressure
Max : Maximum
mech : Mechanical
Min : Minimum
Mix : Mixture
MP : Methanation process
NG : Natural gas
out : Outlet
P : Pump
rev : Revision
s : Steam
ST : Steam turbine
Turb : Turbine

References

[1] Renewable 2019 – International Energy Agency, *https://www.iea.org/reports/renewables-2019* (accessed 19.12).
[2] M. Aneke and M. Wang, Energy storage technologies and real life applications–A state of the art review, *Applied Energy*, 179 (2016) 350-377.
[3] H. Zhao, Q. Wu, S. Hu, H. Xu and C. N. Rasmussen, Review of energy storage system for wind power integration support, *Applied Energy*, 137 (2015) 545-553.
[4] S. B. Walker, U. Mukherjee, M. Fowler and A. Elkamel, Benchmarking and selection of power-to-gas utilizing electrolytic hydrogen as an energy storage alternative, *International Journal of Hydrogen Energy*, 41 (19) (2016) 7717-7731.
[5] O. Schmidt, A. Gambhir, I. Staffell, A. Hawkes, J. Nelson and S. Few, Future cost and performance of water electrolysis: An expert elicitation study, *International Journal of Hydrogen Energy*, 42 (52) (2017) 30470-30492.
[6] M., Götz, J. Lefebvre, F. Mörs, A. M. Koch, F. Graf, S. Bajohr, R. Reimert and T. Kolb, Renewable power-to-gas: a technological and economic review, *Renewable Energy*, 85 (2016) 1371-1390.
[7] G. Gahleitner, Hydrogen from renewable electricity: an international review of power-to-gas pilot plants for stationary applications, *International Journal of Hydrogen Energy*, 38 (5) (2013) 2039-2061.
[8] A. Ursua, L. M. Gandia and P. Sanchis, Hydrogen production from water electrolysis: current status and future trends, *Proc. of the IEEE*, 100 (2) (2012) 410-426.
[9] A. Lewandowska-Bernat and U. Desideri, Opportunities of power-to-gas technology in different energy systems architectures, *Applied Energy*, 228 (2018) 57-67.
[10] D. Ferrero, M. Gamba, A. Lanzini and M. Santarelli, Power-to-gas hydrogen: techno-economic assessment of processes towards a multi-purpose energy carrier, *Energy Procedia*, 101 (2016) 50-57.
[11] J. Burkhardt, A. Patyk, P. Tanguy and C. Retzke, Hydrogen mobility from wind energy-A life cycle assessment focusing on the fuel supply, *Applied Energy*, 181 (2016) 54-64.
[12] G. Guandalini, S. Campanari and M. C. Romano, Power-to-gas plants and gas turbines for improved wind energy dispatchability: energy and economic assessment, *Applied Energy*, 147 (2015) 117-130.
[13] K. Hashimoto, M. Yamasaki, K. Fujimura, T. Matsui, K. Izumiya, M. Komori, A. A. El-Moneim, E. Akiyama, H. Habazaki, N. Kumagai, A. Kawashima and K. Asami, Global CO_2 recycling-novel materials and prospect for prevention of global warming and abundant energy supply, *Materials Science and Engineering: A*, 267 (2) (1999) 200-206.
[14] K. Hashimoto, N. Kumagai, K. Izumiya, H. Takano and Z. Kato, The production of renewable energy in the form of methane using electrolytic hydrogen generation, *Energy*, Sustainability and Society, 4 (17) (2014).
[15] M. Bailera, P. Lisbona, L. M. Romeo and S. Espatolero, Power to gas projects: Lab, pilot and demo plants for storing renewable energy and CO_2, *Renewable and Sustainable Energy Reviews*, 69 (2019) 292-312.
[16] Power-to-gas (demonstration) projects in Europe, *http://european powertogas.com/projects-in-europe* (accessed 18.12).
[17] M. Bailera, B. Peña, P. Lisbona and L. M. Romeo, Decision making methodology for managing photovoltaic surplus electricity through power to gas: combined heat and power in urban buildings, *Applied Energy*, 228 (2018) 1032-1045.
[18] H. Blanco, W. Nijs, J. Ruf and A. Faaij, Potential of power-to-methane in the EU energy transition to a low carbon system using cost optimization, *Applied Energy*, 232 (2018) 323-340.
[19] M. A. Mac Kinnon, J. Brouwer and S. Samuelsen, The role of natural gas and its infrastructure in mitigating greenhouse gas emissions, improving regional air quality, and renewable resource integration, *Progress in Energy and Combustion Science*, 64 (2018) 62-92.

[20] J. Jones, Balancing act: How can we deal with variability?, *Renewable Energy World*, 14 (6) (2011), https://www.renewableenergyworld.com (accessed 19.09).
[21] R. Walton, Gas-fired combustor upgrades offer flexible counterpart to high renewable output, *Power Engineering* (2019), https://www.power-eng.com (accessed 19.09).
[22] M. Sterner, *Bioenergy and Renewable Power Methane in Integrated 100% Renewable Energy Systems: Limiting Global Warming by Transforming Energy Systems*, Kassel University Press GmbH, Kassel, Germany (2009).
[23] M. Bailera, N. Kezibri, L. M. Romeo, S. Espatolero, P. Lisbona and C. Bouallou, Future applications of hydrogen production and CO_2 utilization for energy storage: hybrid power to gas-oxycombustion power plants, *International Journal of Hydrogen Energy*, 42 (19) (2017) 13625-13632.
[24] D. Prakash and O. Singh, Thermo-economic study of combined cycle power plant with carbon capture and methanation, *Journal of Cleaner Production*, 231 (2019) 529-542.
[25] J. H. Kim, T. S. Kim and S. J. Moon, Development of a program for transient behavior simulation of heavy-duty gas turbines, *Journal of Mechanical Science and Technology*, 30 (12) (2016) 5817-5828.
[26] MathWorks, *MATLAB R2017a* (2017).
[27] J. Isles, *Gas Turbine World 2017 Performance Specs*, 33rd Ed., Pequot Publishing Inc., North Carolina, USA (2017).
[28] Aspen Technology Inc., *Aspen HYSYS Ver. 7.3* (2010).
[29] T. B. Olaf, *A Toolbox for Using MATLAB as an ActiveX/COM Controller for Hysys*, Matlab Central.
[30] ANTONI International Inc., *Titan 130 15MW 50Hz GAS 11000V* (2009), https://www.antoni-intl.com (accessed 19.09).
[31] J. H. Choi, J. H. Ahn and T. S. Kim, Performance of a triple power generation cycle combining gas/steam turbine combined cycle and solid oxide fuel cell and the influence of carbon capture, *Applied Thermal Engineering*, 71 (1) (2014) 301-309.
[32] GE Energy Software, *GateCycle Ver. 6.1.2* (2013).
[33] Solar Turbine Inc., *Titan 130 Gas Turbine Generator Set Data Sheet* (2009), http://s7d2.scene7.com (accessed 18.12).
[34] C. A. Palmer and M. R. Erbes, *Simulation Methods used to Analyze the Performance of the GE PG6541B Gas Turbine Utilizing Low Heating Value Fuels*, American Society of Mechanical Engineers (1994) Report No.: CONF-941024-.
[35] D. W. Kang, H. J. Jang and T. S. Kim, Using compressor discharge air bypass to enhance power generation of a steam-injected gas turbine for combined heat and power, *Energy*, 76 (2014) 390-399.
[36] T. L. Bergman, F. P. Incropera, D. P. DeWitt and A. S. Lavine, *Fundamentals of Heat and Mass Transfer*, 6th Ed., John Wiley & Sons, Hoboken, USA (2013).
[37] D. H. Cooke, Modeling of off-design multistage turbine pressures by Stodola's ellipse. *Energy Incorporated PEPSE User's Group Meeting*, Richmond, Virginia, USA (1983).
[38] L. E. Øi, T. Bråthen, C. Berg, S. K. Brekne, M. Flatin, R. Johnsen, I. G. Moen and E. Thomassen, Optimization of configurations for amine based CO_2 absorption using Aspen HYSYS, *Energy Procedia*, 51 (2014) 224-233.
[39] H. Li and J. Yan, Preliminary study on CO_2 processing in CO_2 capture from oxy-fuel combustion, *Proc. of ASME Turbo Expo*, Montreal, Canada (2007) 353-361.
[40] K. Ghaib and F. Z. Ben-Fares, Power-to-Methane: A state-of-the-art review, *Renewable and Sustainable Energy Reviews*, 81 (1) (2018) 433-446.
[41] O. S. Buchholz, A. G. J. van der Ham, R. Veneman, D. W. F. Brilman and S. R. A. Kersten, Power-to-gas: storing surplus electrical energy. A design study, *Energy Procedia*, 63 (2014) 7993-8009.
[42] J. Kopyscinski, T. J. Schildhauer and S. M. A. Biollaz, Production of synthetic natural gas (SNG) from coal and dry biomass-A technology review from 1950 to 2009, *Fuel*, 89 (8) (2010) 1763-1783.
[43] E. I. Koytsoumpa and S. Karellas, Equilibrium and kinetic aspects for catalytic methanation focusing on CO_2 derived Substitute Natural Gas (SNG), *Renewable and Sustainable Energy Reviews*, 94 (2018) 536-550.

Dong Hyeok Won received his M.S. degree from the Dept. of Mechanical Engineering, Inha University, in 2019 and is currently working at mechanical engineering team, Samsung Engineering. His research interests include design and analysis of advanced power plant systems.

Min Jae Kim received his Ph.D. degree from the Dept. of Mechanical Engineering, Inha University, in 2019 and is currently researcher at the R&D Center of Doosan Heavy Industries and Construction. His research interests include design and analysis of advanced power plant systems.

Jae Hong Lee received his B.S. degree from the Dept. of Mechanical Engineering, Inha University, in 2015 and is currently a Ph.D. student in the same department. His research interests include performance analysis and diagnosis of gas turbine power plants.

Tong Seop Kim received his Ph.D. degree from Dept. of Mechanical Engineering, Seoul National University in 1995. He has been with Dept. of Mechanical Engineering, Inha University since 2000. His research interests include design, analysis and diagnosis of advanced energy systems including gas/steam turbine based power plants.